Springer

Journal of
Mechanical
Science and
Technology

Journal of Mechanical Science and Technology 23 (2009) 3459~3470

www.springerlink.com/content/1738-494x
DOI 10.1007/s12206-009-1007-y

Rotor profile design in a hypogerotor pump †

Soon-Man Kwon*, Han Sung Kang and Joong-Ho Shin

Department of Mechanical Design and Manufacturing Engineering, Changwon National University, 9 Sarim-dong, Changwon, Kyongnam 641-773, Republic of Korea

(Manuscript Received May 2, 2008; Revised October 20, 2008; Accepted August 24, 2009)

Abstract

A geometric approach for the outer-rotor profile as a conjugate to the inner-rotor in a hypotrochoidal rotor pump (hypogerotor pump) is proposed by means of the principle of the instantaneous center and the homogeneous coordinate transformation. The inner-rotor profile is defined by the combination of two circular arcs. Next, the radius of curvature of the outer-rotor is derived with the relationships of the trochoid ratio and the inner-rotor tooth size ratio. Then by examining the minimum radius of curvature of the extended hypotrochoidal outer-rotor profile on the convex section, an explicit formula to avoid undercutting in the hypogerotor pump is proposed. It is found that undercut or self-intersection does not occur so long as the minimum value of the radius of curvature on the convex section is not less than zero. Design examples are presented to simulate the operation and to demonstrate the feasibility of the approaches using a computer-aided design program developed on C++ language.

Keywords: Hypogerotor pump; Inner-rotor; Outer-rotor; Instantaneous center; Tip clearance; Trochoid ratio; Inner-rotor tooth size ratio; Radius of curvature; Undercut

1. Introduction

Numerous applications in hydraulic and lubrication systems just require the circulation of the fluid. In such cases low noise emissions and little pressure ripples are more important than highly efficient transmission of energy. The gerotor pump is ideal principle for such applications. Compared to conventional external gear pumps, the suction and pressure connection of the gerotor pump is axial to the driving shaft. This also supports the compact construction. Due to the solid tooth shape, the gerotor pump is resistant to hydraulic and mechanical impact loads. The long durability of the gerotor pump is based on the relatively low sliding speed between the inner and the outer rotor. Furthermore, this pump is characterized by an extremely good smoothness and a low noise level. Designers of engines, compressors, machines tools, tractors, and other equipment requiring hydraulic systems can now build pump components integrally into these mechanisms.

Some important literatures on the basic geometry and its related topics of the gerotor pump can be found: for example, Colbourne [1] proposed a geometry method to find the envelopes of trochoids that perform a planetary motion. Litvin ad Feng [2] used differential geometry to generate the conjugate surfaces of epitrochoidal gearing. Demenego et al. [3] developed a tooth contact analysis (TCA) computer program and discussed avoidance of tooth interference and rapid wearing through modification of the rotor profile geometry of a cycloidal pump whose one pair of teeth is in mesh at every instant. Using the method for determining and tracing the limit curve, Mimmi and Pennacchi [4] obtained transcendental equations for the calculation of the limit dimensions to avoid undercutting. On the while, Ye et al. [5] presented simple explicit formulae by examining the

† This paper was recommended for publication in revised form by Associate Editor Won-Gu Joo

*Corresponding author. Tel.: +82 55 213 3629, Fax.: +82 55 263 5221
E-mail address: smkwon@changwon.ac.kr

radius of curvature on the convex section for calculating the limit dimensions to avoid undercutting in the inner-rotor.

However, most earlier studies focused on the commercially available gerotor pump using the equidistant shortened epitrochoid curve to the authors' best knowledge. To improve the carryover phenomenon of the traditional gerotor design, most recently Hwang and Hsieh [6] presented a geometry design procedure based upon the theories of envelope and conjugate surfaces for the hypotrochoidal gear pump (abbreviated as "hypogerotor pump" in this paper) using the equidistant extended hypotrochoid curve. They also presented non-undercutting conditions of the outer-rotor using the theory of gearing [7]. However, the procedure for obtaining the non-undercutting conditions of [6] is somewhat complicated with the added disadvantages that equations must be solved numerically.

This paper presents the method on rotor profile design of a hypogerotor pump. The outer-rotor profile as a conjugate to the inner-rotor is defined by the principle of the instantaneous center and the homogeneous coordinate transformation in Section 2, and the inner-rotor profile is defined by the combination of two circular arcs in Section 3.

Next, the radius of curvature of the outer-rotor is derived with the relationships of the trochoid ratio and the inner-rotor tooth size ratio in Section 4. Then by examining the minimum radius of curvature of the outer-rotor on the convex section following the methodology of [5], an explicit formula for the limit dimensions to avoid self-intersecting or undercutting is proposed in Section 5. It is found that self-intersection does not occur so long as the minimum value of radius of curvature on the convex section is not less than zero. With the result obtained in this paper, the calculation becomes a much simpler task than that of [6].

Based on developed analytical expressions, some discussions are addressed in Section 6 to demonstrate the feasibility of the approaches.

2. Outer-rotor tooth profile

A hypogerotor pump (see Fig. 1) consists of two main components: an inner-rotor and an outer-rotor that has one more tooth than the inner-rotor. The inner-rotor centerline is positioned at a fixed eccentricity from the centerline of the outer-rotor. As the rotors rotate in the same direction about their respective axes, fluid is drawn into the enlarging chamber up to a maximum volume. As rotation continues, the chamber volume decreases, forcing fluid out of the chamber. This process, used primarily in liquid transportation and many fluid power applications, occurs constantly for each chamber, providing a smooth pumping action.

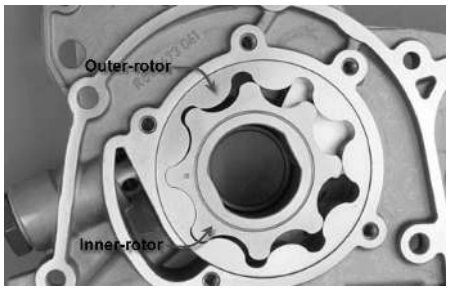

Fig. 1. Typical hypogerotor pump.

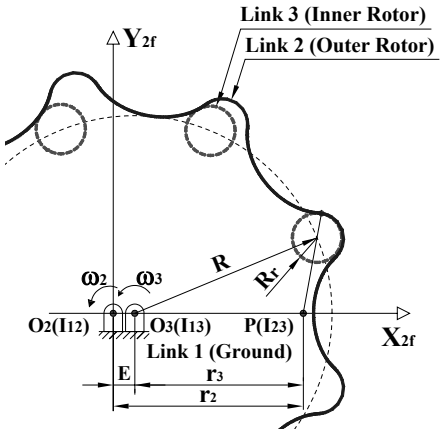

Fig. 2. Instantaneous centers in a hypogerotor pump.

We have displayed a schematic of the hypogerotor pump in Fig. 2. The number of teeth of the inner-rotor is always one less than the outer-rotor, i.e., they have N and $(N+1)$ teeth, respectively. We can choose any shape for the inner-rotor teeth, and the outer-rotor is then generated conjugate to the inner-rotor. We describe here only the inner-rotor having N arcs of circle in the placement of R from its center with the radius of R_r. The center distance between rotors (or eccentricity) is E. It can be regarded kinematically as a mechanism of three-links and three-joints: the frame corresponding to $E=\overline{O_2O_3}$ as Link 1, the outer-rotor as Link 2, and the inner-rotor as Link 3, respectively.

The outer-rotor (Link 2) turns about O_2, and the inner-rotor (Link 3) turns about its center O_3, the angular velocity ratio being $N:(N+1)$. Two points

O_2 and O_3 are permanent instantaneous centers I_{12} and I_{13}, respectively. We will denote the two pitch radii $r_2 = \overline{O_2 I_{23}} = \overline{O_2 P}$ and $r_3 = \overline{O_3 I_{23}} = \overline{O_3 P}$ which are unknowns to be determined below. The magnitude of the velocity $\vec{V}_{23}$ at pitch point I_{23} (P) can be determined by

$$V_{23} = r_2\omega_2 = r_3\omega_3 \tag{1}$$

The angular velocity ratio can be written as

$$\frac{\omega_2}{\omega_3} = \frac{r_3}{r_2} = \frac{N}{N+1} \tag{2}$$

From Eq. (2), we can easily determine the location of the pitch point I_{23} with the aid of relation $r_2 - r_3 = E$ and Kennedy's theorem [8] as follows:

$$r_2 = E(N+1), \quad r_3 = EN \tag{3}$$

Before deriving the profile equation of the outer-rotor, three coordinate systems corresponding to the hypogerotor pump should be defined as shown in Fig. 3: one stationary reference system S_{2f} attached to O_2, and two mobile reference systems S_2 and S_3 attached to O_2 and O_3, respectively. The angles of ϕ_2 and ϕ_3 are profile definition parameters of the reference systems S_2 and S_3, respectively.

In Fig. 3, the contact point is C and the common normal to both rotors passes through the pitch point I_{23}. Therefore, the mesh point ${}^3C$ in S_3-coordinate system and the corresponding leaning angle ψ can be determined as below:

$$\begin{aligned} {}^3x_C &= R + R_r\cos\psi \\ {}^3y_C &= R_r\sin\psi \end{aligned} \tag{4}$$

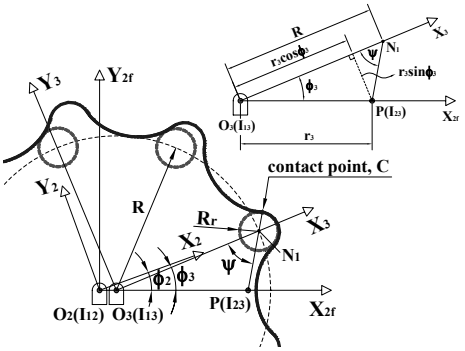

Fig. 3. Three coordinate systems for outer-rotor profile definition.

$$\psi = \tan^{-1}\left(\frac{\sin\phi_3}{\mu - \cos\phi_3}\right) \tag{5}$$

where the parameter of $\mu = R/r_3$ is used consistently throughout this paper and is referred to as the *trochoid ratio*. It is recommended that the designer of the hypogerotor pump should adopt the curtate hypotrochoid curves (i.e. $\mu > 1$) to avoid self-intersection phenomenon.

The origin of coordinate system does not coincide with that of the outer-rotor in Eq. (4). In such a case the coordinate transformation may be used based on the application of homogeneous coordinates and 4×4 matrices that describe separately rotation about a stationary axis and displacement of one coordinate system with respect to the other [7]. For the homogeneous coordinate transformation from the contact point of ${}^3C$ in S_3-reference system to that of ${}^2C$ in S_2-reference system, the following matrix equation is defined:

$${}^2C = \boldsymbol{M}_{2,3}\,{}^3C = \boldsymbol{M}_{2,2f}(\phi_2)\boldsymbol{M}_{2f,3}(\phi_3)\,{}^3C \tag{6}$$

where the matrix $\boldsymbol{M}_{i,j}$ describes transformation from S_j-system to S_i-system, and

$$\boldsymbol{M}_{2,2f}(\phi_2) = \begin{bmatrix} \cos\phi_2 & \sin\phi_2 & 0 & 0 \\ -\sin\phi_2 & \cos\phi_2 & 0 & 0 \\ 0 & 0 & 1 & 0 \\ 0 & 0 & 0 & 1 \end{bmatrix} \tag{7}$$

$$\boldsymbol{M}_{2f,3}(\phi_3) = \begin{bmatrix} \cos\phi_3 & -\sin\phi_3 & 0 & E \\ \sin\phi_3 & \cos\phi_3 & 0 & 0 \\ 0 & 0 & 1 & 0 \\ 0 & 0 & 0 & 1 \end{bmatrix} \tag{8}$$

$${}^3C = \begin{bmatrix} R + R_r\cos\psi & R_r\sin\psi & 0 & 1 \end{bmatrix}^T \tag{9}$$

where the superscript T in Eq. (9) means the transpose of the matrix.

The resulting expression of Eq. (6) is

$${}^2C = \begin{bmatrix} (R + R_r\cos\psi)\cos(\phi_2 - \phi_3) \\ +R_r\sin\psi\sin(\phi_2 - \phi_3) + E\cos\phi_2 \\ -(R + R_r\cos\psi)\sin(\phi_2 - \phi_3) \\ +R_r\sin\psi\cos(\phi_2 - \phi_3) - E\sin\phi_2 \\ 0 \\ 1 \end{bmatrix} \tag{10}$$

From Eq. (2), we have the following relation,

$$\frac{\omega_2}{\omega_3}=\frac{d\phi_2/dt}{d\phi_3/dt}=\frac{\phi_2}{\phi_3}=\frac{N}{N+1} \tag{11}$$

If we define ϕ by the generated parameter of output motion, we can obtain $\phi_2 = N\phi$ and $\phi_3 = (N+1)\phi$. Substituting these relations into Eq. (10) leads to the following lobe profile parametric equations in S_2-reference system:

$$^2x_C = R\cos\phi + R_r\cos(\phi+\psi) + E\cos(N\phi) \tag{12a}$$

$$^2y_C = R\sin\phi + R_r\sin(\phi+\psi) - E\sin(N\phi) \tag{12b}$$

where

$$\psi = \tan^{-1}\left[\frac{\sin(N+1)\phi}{\mu-\cos(N+1)\phi}\right],\ (0\le\phi\le 2\pi) \tag{13}$$

The real profiles are manufactured with technological gaps due to many practical considerations, such as precision of machining tools, prevention of jamming conditions, and application of lubricants. Although gear teeth gaps are inevitable, they may lead to fluid losses and occurrence of additional dynamic forces, decrease stability and increase noise and vibration, especially at high speeds. The requirement for a proper tip clearance is a trade-off problem.

The equidistant curve principle is applied to realize the proper tolerances for the outer-rotor profile, and as a consequence, the offset profile to the ideal one of Eqs. (12) is obtained.

This equidistant offset profile will be generated as equidistant of Eqs. (12) with equidistant radius larger or smaller than the theoretical one (R_r) by a tip clearance, δ_t, as follows:

$$^2x_C(\delta_t) = R\cos\phi + (R_r+\delta_t)\cos(\phi+\psi) + E\cos(N\phi) \tag{14a}$$

$$^2y_C(\delta_t) = R\sin\phi + (R_r+\delta_t)\sin(\phi+\psi) - E\sin(N\phi) \tag{14b}$$

These give a uniformly enlarged equidistant curve (Fig. 4) when $\delta_t > 0$. On the other hand, these give a uniformly contracted equidistant curve (Fig. 5) for $\delta_t < 0$. Eqs. (14) are the equations of the profile on the non-ideal outer-rotor.

We can observe that Eqs. (14) can be degenerated into the well-known standard hypotrochoid equations in the forms for the case when $\delta_t = -R_r$ (see Fig. 5):

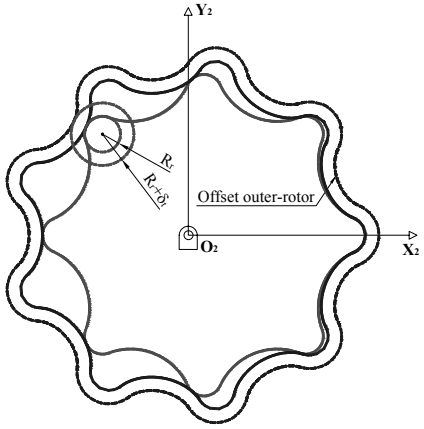

Fig. 4. Equidistant offset outer-rotor lobe profile (dashed line).

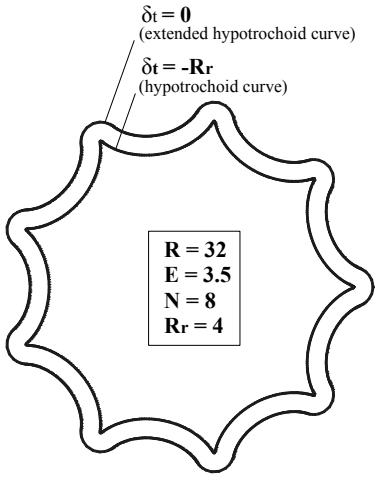

Fig. 5. Outer-rotor shape in case of $\delta_t = -R_r$.

$$^2x_C = R\cos\phi + E\cos(N\phi) \tag{15a}$$

$$^2y_C = R\sin\phi - E\sin(N\phi) \tag{15b}$$

Next, we consider the outer-rotor rotated by the amount of θ_2 (see Fig. 6) for the sake of generalization. In that case, we can describe the outer-rotor profile in the stationary S_{2f}-reference system as follows:

$$^{2f}C = \boldsymbol{M}_{2f,2}(\theta_2)\ {}^2C \tag{16}$$

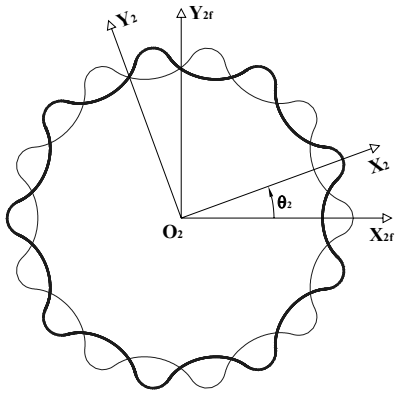

Fig. 6. Outer-rotor profile in case of rotation of θ_2 .

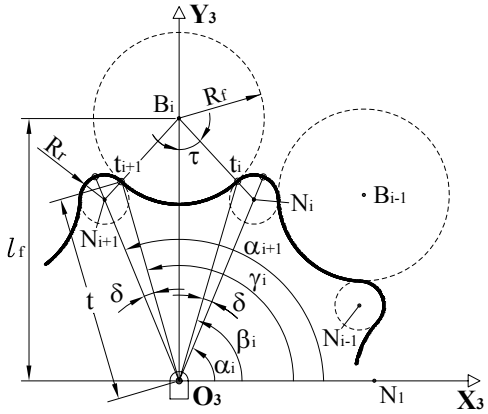

Fig. 7. Definition of inner-rotor parameters.

where

$$\boldsymbol{M}_{2f,2}(\theta_2)=\begin{bmatrix}\cos\theta_2 & -\sin\theta_2 & 0 & 0\\ \sin\theta_2 & \cos\theta_2 & 0 & 0\\ 0 & 0 & 1 & 0\\ 0 & 0 & 0 & 1\end{bmatrix} \tag{17}$$

$${}^{2}C=\begin{bmatrix}R\cos\phi+(R_r+\delta_t)\cos(\phi+\psi)+E\cos(N\phi)\\ R\sin\phi+(R_r+\delta_t)\sin(\phi+\psi)-E\sin(N\phi)\\ 0\\ 1\end{bmatrix} \tag{18}$$

The outer-rotor profile in S_{2f} -reference system becomes

$${}^{2f}x_C=R\cos(\phi+\theta_2)+(R_r+\delta_t)\cos(\phi+\psi+\theta_2)+E\cos(N\phi-\theta_2) \tag{19a}$$

$${}^{2f}y_C=R\sin(\phi+\theta_2)+(R_r+\delta_t)\sin(\phi+\psi+\theta_2)-E\sin(N\phi-\theta_2) \tag{19b}$$

3. Inner-rotor tooth profile and flow rate

The inner-rotor (see Figs. 7 and 8) can be defined by the combination of two circular arcs: inner-rotor teeth circular arcs of Section I ($\alpha_i \le \Phi \le \beta_i$ and $\gamma_i \le \Phi \le \alpha_{i+1}$), and fillet circular arcs of Section II ($\beta_i \le \Phi \le \gamma_i$). The position angles shown in Fig. 7 are

$$\alpha_i=\angle\left(X_3,\overline{O_3N_i}\right)=\frac{2\pi}{N}(i-1),(i=1,2,3,\cdots,N) \tag{20a}$$

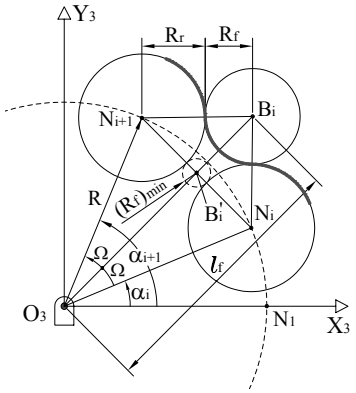

Fig. 8. Schematic for determination of l_f .

$$\beta_i=\angle\left(X_3,\overline{O_3t_i}\right)=\alpha_i+\delta \tag{20b}$$

$$\gamma_i=\angle\left(X_3,\overline{O_3t_{i+1}}\right)=\alpha_{i+1}-\delta \tag{20c}$$

Here the section discrimination angle δ can be determined from $\Delta O_3t_{i+1}N_{i+1}$ of Fig. 7 as

$$\delta=\cos^{-1}\left(\frac{t^2+R^2-R_r^2}{2tR}\right) \tag{21}$$

where

$$t=\sqrt{l_f^2+R_f^2-2l_fR_f\cos\tau} \tag{22a}$$

$$\cos\tau=\frac{l_f^2+\left(R_r+R_f\right)^2-R^2}{2l_f\left(R_r+R_f\right)} \tag{22b}$$

$$l_f=\overline{O_3B_i}=R\cos\Omega+\sqrt{\left(R\cos\Omega\right)^2-R^2+\left(R_r+R_f\right)^2} \tag{22c}$$

and $\Omega=(\alpha_{i+1}-\alpha_i)/2=\pi/N$.

Eq. (22a) is obtained by $\Delta O_3B_it_i$, Eq. (22b) by $\Delta O_3N_iB_i$, and Eq. (22c) by $\Delta O_3N_{i+1}B_i$ or $\Delta O_3N_iB_i$ of Fig. 8, respectively.

The circular arc equations of Section I (Fig. 9) and Section II (Fig. 10) in the stationary S_{3f} -reference system can be written, respectively, as follows:

$$\begin{aligned}&\left({}^{3f}x_D-R\cos(\alpha_i+\theta_3)\right)^2\\&+\left({}^{3f}y_D-R\sin(\alpha_i+\theta_3)\right)^2=R_r^2\end{aligned} \tag{23a}$$

$$\begin{aligned}&\left({}^{3f}x_D-l_f\cos(\alpha_i+\Omega+\theta_3)\right)^2\\&+\left({}^{3f}y_D-l_f\sin(\alpha_i+\Omega+\theta_3)\right)^2=R_f^2\end{aligned} \tag{23b}$$

where the angle θ_3 represents the rotation angle of the inner-rotor. The relation between the rotation angles of the rotors is $\theta_2/\theta_3=N/(N+1)$.

The S_{3f} -coordinates of point D in Figs. 9 and 10 are

$${}^{3f}x_D=r(\Phi)\cos(\Phi+\theta_3) \tag{24a}$$

$${}^{3f}y_D=r(\Phi)\sin(\Phi+\theta_3) \tag{24b}$$

where

$$\Phi=\angle\left(X_3,\overline{O_3C}\right)=\tan^{-1}\left(\frac{{}^{3f}y_C(\phi)}{{}^{3f}x_C(\phi)}\right)-\theta_3 \tag{25a}$$

$${}^{3f}x_C={}^{2f}x_C-E\ ,\quad {}^{3f}y_C={}^{2f}y_C \tag{25b}$$

Here we defined the position angle Φ as Eq. (25a) (see Fig. 11) in order to calculate the chamber area easily. It allows the same position data between rotors. Substituting Eqs. (24) into Eqs. (23), we find

$$\begin{aligned}r(\Phi)&=R\cos(\Phi-\alpha_i)\\&\quad+\sqrt{R_r^2-R^2+R^2\cos^2(\Phi-\alpha_i)},\\&\quad(\alpha_i\le\Phi\le\beta_i)\end{aligned} \tag{26a}$$

$$\begin{aligned}r(\Phi)&=l_f\cos(\Phi-(\alpha_i+\Omega+\theta_3))\\&\quad-\sqrt{R_f^2-l_f^2+l_f^2\cos^2(\Phi-(\alpha_i+\Omega+\theta_3))},\\&\quad(\beta_i\le\Phi\le\gamma_i)\end{aligned} \tag{26b}$$

$$\begin{aligned}r(\Phi)&=R\cos(\Phi-\alpha_{i+1})\\&\quad+\sqrt{R_r^2-R^2+R^2\cos^2(\Phi-\alpha_{i+1})},\\&\quad(\gamma_i\le\Phi\le\alpha_{i+1})\end{aligned} \tag{26c}$$

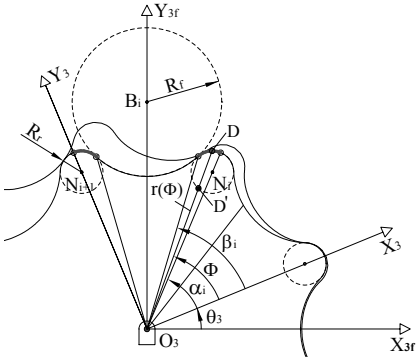

Fig. 9. Section I of inner-rotor tooth profile in S_{3f} -system.

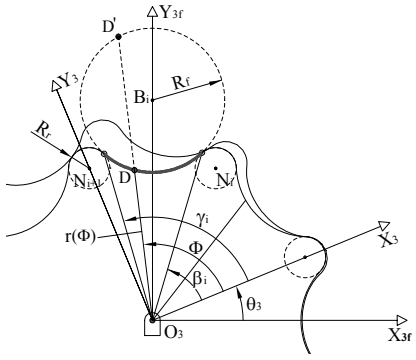

Fig. 10. Section II of inner-rotor tooth profile in S_{3f} -system.

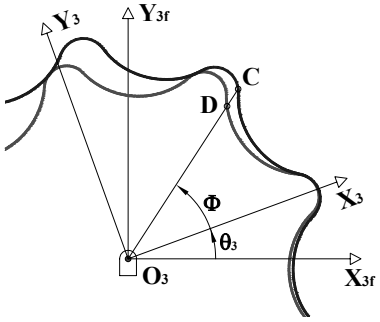

Fig. 11. Definition of generated parameter Φ .

Once the generated shape and conjugate shape are known, the volume displaced by the working pocket, as this pocket goes through a complete cycle from maximum volume ($A_{\max}\times H$) to minimum volume ($A_{\min}\times H$), can be determined. Here $A_{\max}$, $A_{\min}$ and H represent the maximum chamber area, the minimum chamber area and the rotor thickness, respectively.

For this goal, the evaluation procedure of the i-th chamber area, A_i , at any instant should be preceded.

It can be carried out from Fig. 12 numerically as follows:

$$A_i = \frac{1}{2}\int_{\Phi_{0i}}^{\Phi_{ni}} \left(C_k^2 - D_k^2\right) d\Phi \approx \frac{1}{2}\sum_{k=1}^{n}\left(C_k^2 - D_k^2\right)\Delta\Phi_k \quad (27)$$

where

$$C_k^2 = {}^{3f}x_C^2\left(\phi_{ki}\right) + {}^{3f}y_C^2\left(\phi_{ki}\right) \quad (28a)$$

$$D_k^2 = {}^{3f}x_D^2\left(\Phi_{ki}\right) + {}^{3f}y_D^2\left(\Phi_{ki}\right) \quad (28b)$$

$$\Delta\Phi_k = \Phi_{ki} - \Phi_{(k-1)i} \quad (28c)$$

and Φ_{0i} and Φ_{ni} are the start and the end position angles of the i-th chamber, respectively. These angles are calculated from the schematic of Fig. 13 for determination of contact angle $\theta_c(i)$,

$$\Phi_{0i} = \theta_c(i) = \tan^{-1}\left(\frac{Y_c(i)}{X_c(i)}\right) - \theta_3 \quad (29a)$$

$$\Phi_{ni} = \theta_c(i+1) = \tan^{-1}\left(\frac{Y_c(i+1)}{X_c(i+1)}\right) - \theta_3 \quad (29b)$$

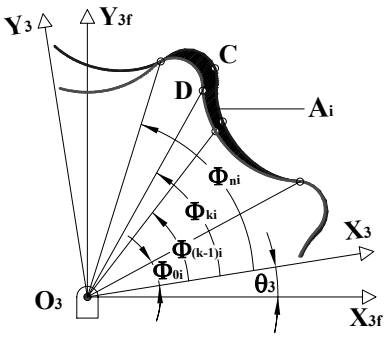

Fig. 12. Schematic for chamber area.

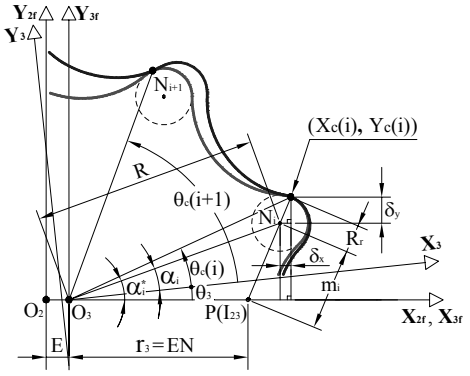

Fig. 13. Schematic for determination of contact angle, θ_c.

where

$$X_c(i) = R\cos\alpha_i^*\left(1 + \frac{R_r}{m_i}\right) - \frac{r_3 R_r}{m_i} \quad (30a)$$

$$Y_c(i) = R\sin\alpha_i^*\left(1 + \frac{R_r}{m_i}\right) \quad (30b)$$

$$m_i = \overline{I_{23}N_i} = r_3\sqrt{\mu^2 + 1 - 2\mu\cos\alpha_i^*} \quad (30c)$$

and $\alpha_i^* = \alpha_i + \theta_3$.

To determine the working area of $\Delta A = A_{\max} - A_{\min}$ with the aid of Eq. (27), it should be noted that both $A_{\max}$ and $A_{\min}$ occur simultaneously at $\theta_3 = (2j-1)\pi/N$ (where $j = 1, 2, \cdots, N$) for the case when N is even number, while $A_{\max}$ at $\theta_3 = 2(j-1)\pi/N$ and $A_{\min}$ at $\theta_3 = (2j-1)\pi/N$, respectively, for the case when N is odd number.

Since $A_{\max}$ or $A_{\min}$ occur N times for every rotational turn of the inner-rotor, the specific flow rate V_{th} (or theoretical displacement per unit revolution) can be determined as $V_{th} = \Delta A \times H \times N$.

Therefore, the oil flow rate of the hypogerotor pump is calculated as

$$q = \eta_V \times V_{th} \times rpm \quad (31)$$

where η_V is the volumetric efficiency mainly depending on tip clearance and face clearance, and (rpm) is the rotational speed of the inner-rotor.

4. Radius of curvature for outer-rotor

During the design stage of the hypogerotor pump, the size (R_r) and the placement (R) of the cylindrical inner-rotor teeth are those of important dimensions. If R_r is larger than a maximum value or R is less than a minimum value, then the enveloped tooth profile of the outer rotor will self-intersect (see Fig. 14). The tooth profile of the outer-rotor will therefore be undercut. This will produce backlash between rotors during running and become a potential problem, e.g., a decrease in volumetric efficiency. It is therefore important to calculate limit dimensions to avoid undercutting on the outer-rotor when designing the geotor pump. It is also well known that the wear rate can be reduced by increasing the radius of curvature of the lobes. The radius of curvature is a function of the size and the placement of the inner-rotor teeth which generate the lobe shape.

As is well known, the formula for the radius of curvature of a parametric curve is

$$\rho = \frac{\left[\left(x'\right)^2 + \left(y'\right)^2\right]^{3/2}}{x''y' - x'y''} \tag{32}$$

where (x , y) are coordinates of the parametric curve, (x' , y') and (x'' , y'') are the first and the second derivatives of (x , y) with respect to parameter, respectively. If $\rho > 0$ in Eq. (32), then the location of the center of curvature is to the right of the path (i.e., convex profile).

If the mesh points of ${}^2C$ in Eqs. (12) are differentiated with respect to ϕ, then the resulting formula for the radius of curvature of the tooth profile of the outer-rotor will be very complicated because of the term of ψ. It will be impossible to obtain directly an explicit formula. However, it will be overcome with the introduction of the radius of curvature for the standard hypotrochoid curve (see Fig. 5). When $\delta_t = -R_r$ in Eqs. (14), we can obtain the standard hypotrochoid curve as in Eqs. (15). With the radius of curvature ρ_{N_1} of the standard hypotrochoid curve, the radius of curvature of the outer-rotor path (extended hypotrochoid curve) traced by the mesh point ${}^2C$, at a specified input position ϕ, can be found as

$$\rho = \rho_{N_1} - R_r \tag{33}$$

To find ρ_{N_1}, we consider Eqs. (14) and (15), i.e., $x = {}^2x_C(\delta_t = -R_r)$ and $y = {}^2y_C(\delta_t = -R_r)$.

Substituting Eqs. (15) into Eq. (32) yields a simpler formula with parameter of $\phi_3 = (N+1)\phi$ as follows:

$$\rho = \frac{r_3\left(\mu^2 + 1 - 2\mu\cos\phi_3\right)^{3/2}}{N - \mu^2 - \mu(N-1)\cos\phi_3} - R_r \tag{34a}$$

or in the normalized form of radius of curvature

$$\rho^* = \frac{\rho}{R} = \frac{\left(\mu^2 + 1 - 2\mu\cos\phi_3\right)^{3/2}}{\mu\left[N - \mu^2 - \mu(N-1)\cos\phi_3\right]} - \lambda \tag{34b}$$

where $\lambda = R_r / R$ is the *inner-rotor tooth size ratio*.

The transition between concave and convex portions results in the radius of curvature becoming infinite. This inflection point will occur in the hypotrochoidal path when the denominator in Eqs. (34) tends to zero:

$$N - \mu^2 - \mu(N-1)\cos\phi_3 = 0 \tag{35a}$$

or

$$\cos\phi_3 = \frac{N - \mu^2}{\mu(N-1)} \tag{35b}$$

Since N and μ are positive and real values, then $\cos\phi_3 > 0$, i.e., $0 \le \phi_3 \le \pi/2$. Therefore, an inflection point will occur when

$$0 < \frac{N - \mu^2}{\mu(N-1)} \le 1 \tag{36}$$

5. Non-undercut condition for outer-rotor

To demonstrate the interference (or self-intersecting) phenomenon, two outer-rotors are depicted simultaneously in Fig. 14. The same design parameters (R =32, N =8, E =3.5) have been used in Fig. 14, with the exception of R_r (equal to 4 in the smaller rotor and 20 in the larger rotor). Shown in Fig. 15 is the relationship between radius of curvature ρ of the tooth profile and the generated parameter ϕ_3. From Fig. 15, we can observe that the radius R_r of the inner-rotor tooth increases, then ρ decreases. If R_r is larger than a limit value, the minimum radius of curvature on the convex section will be negative and the tooth profile of the outer-rotor will be intersecting. This will produce backlash between the outer-rotor and inner-rotor during running. To avoid this self-intersecting, the point with zero radius of curvature must be avoided, i.e., the minimum value of ρ of the tooth profile on the convex section should not be less than zero.

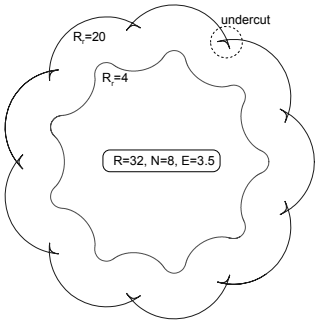

Fig. 14. Outer-rotor profile design example for showing undercut.

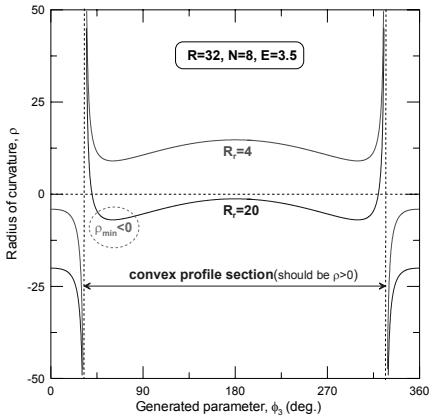

Fig. 15. Radius of curvature for the design example.

In order to calculate $\rho_{\min}$ on the convex section, Eqs. (34) are differentiated with respect to ϕ_3 and setting the result equal to zero. After rearranging, the equation is observed to be of the form

$$A \times B \times C = 0 \tag{37}$$

where

$$A = \sin\phi_3 \tag{38a}$$

$$B = \sqrt{\mu^2 + 1 - 2\mu\cos\phi_3} \tag{38b}$$

$$C = 2N + 1 - \mu^2(N+2) - \mu(N-1)\cos\phi_3 \tag{38c}$$

It is clear from Eq. (37) that there are three distinct cases where stationary curvature in the hypotrochoidal path could occur: when $A = 0$, and/or $B = 0$, and/or $C = 0$. As it is important to understand each case, they are presented now in some detail.

(*Case 1*). Consider $A = 0$; i.e., $\sin\phi_3 = 0$.

The values of the generated parameter which satisfy this condition are $\phi_3 = 0$ or $\phi_3 = \pi$. Substituting $\phi_3 = 0$ and $\phi_3 = \pi$ into Eq. (34a) and simplifying, the first and the second local extrema are

$$\rho_1 = \rho_{\phi_3=0} = -\frac{r_3(\mu-1)^2}{\mu+N} - R_r \tag{39}$$

$$\rho_2 = \rho_{\phi_3=\pi} = \frac{r_3(\mu+1)^2}{N-\mu} - R_r \tag{40}$$

These first and second local extrema are the radius of curvature of the initial generated point at the bottom of the lobe for internal contact and the radius of curvature occurring at the top of the lobe for internal contact, respectively.

(*Case 2*). Consider $B = 0$; i.e., Eq. (38b) may be written as

$$\sqrt{\mu^2 + 1 - 2\mu\cos\phi_3} = 0 \tag{41}$$

For Eq. (41) to be a possible solution, the relationship between the trochoid ratio and the generating angle is

$$\mu = \cos\phi_3 \pm \sqrt{\cos^2\phi_3 - 1} \tag{42}$$

Since $\mu > 0$, then the only value of ϕ_3 which satisfy this condition is $\phi_3 = 0$. Substituting this value into Eq. (42) gives $\mu = 1$. Then substituting $\mu = 1$ into Eq. (39), we see that the first local extremum $\rho_1 = (\rho_{N_i} = 0) - R_r$. This defines a cusp in the path of point N_i and is a special case which may not be a practical solution.

(*Case 3*). Consider $C = 0$; i.e., Eq. (38c) may be written as

$$2N + 1 - \mu^2(N+2) - \mu(N-1)\cos\phi_3 = 0 \tag{43a}$$

or

$$\cos\phi_3 = \frac{2N + 1 - \mu^2(N+2)}{\mu(N-1)} \tag{43b}$$

As $|\cos\phi_3| \le 1$, the third local extremum occurs when the trochoid ratio is

$$1 < \mu < \frac{2N+1}{N+2} \tag{44}$$

This equation is the most general result for the trochoid ratio of a practical hypotrochoidal gerotor.

Substituting Eq. (43b) into Eqs. (34) and simplifying, the third local extremum is

$$\rho_3 = r_3\left(\frac{3}{N-1}\right)^{3/2}\sqrt{(\mu^2-1)(N+1)} - R_r \tag{45a}$$

or

$$\rho_3^* = \frac{1}{\mu}\left(\frac{3}{N-1}\right)^{3/2}\sqrt{(\mu^2-1)(N+1)} - \lambda \tag{45b}$$

If the trochoid ratio satisfies Eq. (44) then all three local extrema will occur on the path. However, if the trochoid ratio $\mu \geq (2N+1)/(N+2)$, then only the first and second local extrema can occur on the path.

As stated before, to avoid self-intersecting, the value of $\rho_{\min}$ on the convex section should not be less than zero. Setting $\rho_3 = 0$ results in an explicit formula for calculating the maximum value of $\lambda_{\max}$ of the inner-rotor tooth size ratio to avoid undercutting on the outer-rotor

$$\lambda_{\max} = \frac{(R_r)_{\max}}{R} = \frac{1}{\mu}\left(\frac{3}{N-1}\right)^{3/2}\sqrt{(\mu^2-1)(N+1)} \tag{46}$$

If R_r has been determined beforehand, then the minimum distance $R_{\min}$ can be calculated by the following explicit formula derived from Eq. (46):

$$R_{\min} = \sqrt{\frac{R_r^2(N-1)^3}{27(N+1)} + r_3^2} \tag{47}$$

Using Eqs. (46) and (47) it is very easy to calculate limit dimensions. For an example, if the design parameters are given by R =32, N =8, and E =3.5 as in Figs. 14 and 15, the maximum inner-rotor tooth radius to avoid undercutting is $(R_r)_{\max}$ =13.04.

6. Discussion

Based on the obtained results, a computer-aided package "HypoGerotor V2.0" has been developed to design the hypogerotor pump using C^{++} language in connection with OpenGL. This CAD program has the characteristics of the graphic user interface and the simulation of the real operation for the hypogerotor pump.

To validate of the proposed approach, we revisit the existing result of Hwang and Hsieh [6]. They presented two special cases as in Table 1.

These two cases have no undercutting on the profiles, causing the design values of R_r to be lower than their $(R_r)_{\max}$ values. As can be shown in Fig. 16, our results are in exact agreement with those of [6].

According to the result of Saenko and Gorbatyuk [9], the theoretical displacement of the epitrochoidal gerotor pump is approximately evaluated as $V_{th} \approx 4\pi E(R - R_r)H$. In other words, V_{th} increases in that pump with the increase of R and E, but decreases with the increase of R_r. However, it should be noted that the theoretical displacement V_{th} of the hypogerotor increases as increasing of R, E and R_r. This trend is somewhat different from that of the epitrochoidal gerotor pump.

Table 1. Design parameters for comparison.

	Parameters given in [6]	Design constraint
Case 1	N=4, R=30, E=6.9, R_r=4.2	$(R_r)_{max}$=26.29
Case 2	N=6, R=20, E=3.0, R_r=3.0	$(R_r)_{max}$ =10.72

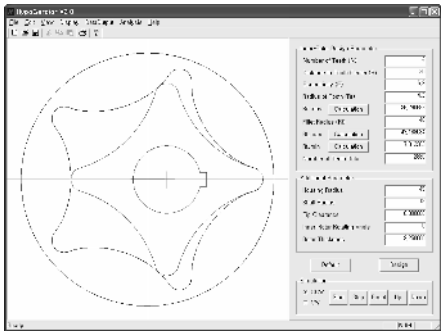

(a) Case 1

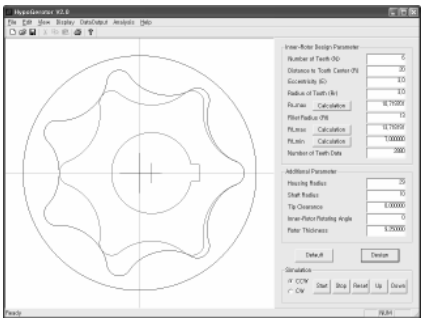

(b) Case 2

Fig. 16. Comparison with the existing result [6].

The trochoid ratio μ for all commercially available hypogerotor pump will have a value that satisfies Eq. (44); i.e. the local extremum given by Eqs. (45) is the most common minimum radius of curvature on the convex section of the tooth profile. For an illustrative purpose, the maximum inner-rotor tooth size ratio of Eq. (46) is graphically represented in Fig. 17 with the variation of the trochoid ratio under the limit condition of Eq. (44). From Fig. 17, we can observe that (a) permissible $\lambda_{\max}$ increases as μ increases; (b) permissible $\lambda_{\max}$ decreases with the increase of N; and (c) the range of μ for practical purpose is getting wider as N increases because of the limit condition of Eq. (44).

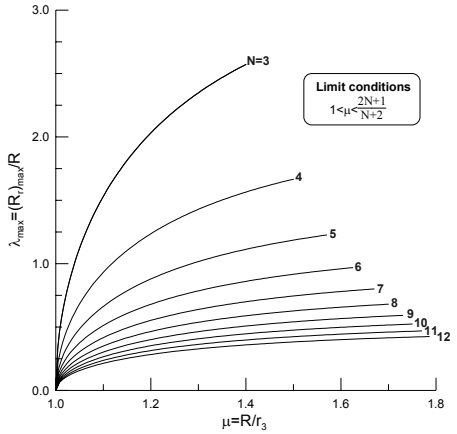

Fig. 17. Maximum tooth size ratio with the variation of trochoid ratio.

Besides, in the hypogerotor pump design, to avoid contact with or interference between the two neighbor inner-rotor teeth or existence of the fillet radius of $\left(R_f\right)_{\min}$, the maximum permissible value of the inner-rotor tooth size ratio is denoted as λ_c and the inner-rotor tooth radius or the inner-rotor tooth size ratio may be constrained by the following relation (see Fig. 8):

$$0 < R_r < R\sin\Omega \tag{48a}$$

$$0 < \lambda < \lambda_c = \sin\Omega \tag{48b}$$

However, because Eqs. (48) only determine the design range of the inner-rotor tooth size, Eq. (46) (the equation of undercutting) must be employed to the feasible design.

7. Conclusions

The exact outer-rotor profile and some explicit formulae for the limit dimensions to avoid undercutting in the hypogerotor pump have been obtained by the principle of the instantaneous center, and by examining the minimum radius of curvature on the convex section of the lobe profile, respectively. The following conclusions can be drawn:

(1) The parametric lobe profile equations of the outer-rotor in a hypogerotor pump are analyzed and obtained by the principle of the instantaneous center. The present results are easy to understand and exact.

(2) Simple explicit formulae for no interference conditions are presented by examining the minimum radius of curvature on the convex section of the outer-rotor profile.

(3) The developed design methodology has been successfully applied to the hypogerotor pump using a computer-aided program, and some examples have been presented to verify the validity of the developed methodology.

Acknowledgment

This research is financially supported by Changwon National University in 2009-2010.

References

[1] J. R. Colbourne, The geometry of trochoid envelopes and their application in rotary pumps, *Mechanism and Machine Theory* 4 (1974) 421-435.

[2] F. L. Litvin and P. H. Feng, Computerize design and generation of cycloidal gearing, *Mechanism and Machine Theory* 31 (1996) 891-911.

[3] A. Demenego, D. Vecchiato, F. L. Litvin, N. Nervegna and S. Manco, Design and simulation of meshing of a cycloidal pump, *Mechanism and Machine Theory* 37 (2002) 311-332.

[4] G. C. Mimmi and P. E. Pennacchi, Non-undercutting conditions in internal gears, *Mechanism and Machine Theory* 35 (2000) 477-490.

[5] Z. Ye, W. Zhang, Q. Huang and C. Chen, Simple explicit formulae for calculating limit dimensions to avoid undercutting in the rotor of a cycloid rotor pump, *Mechanism and Machine Theory* 41 (2006) 405-414.

[6] Y.-W. Hwang and C.-F. Hsieh, Geometry design using hypotrichoid and nonundercutting conditions for an internal cycloidal gear, Transactions of the *ASME, Journal of Mechanical Design* 129 (2007) 413-420.

[7] F. L. Litvin, *Gear geometry and Applied Theory*. PTR Prentice Hall, Englewood Cliffs, (1994).

[8] J. E. Shigley and Jr. J. J. Uicker, *Theory and Machines and Mechanisms*. McGraw-Hill, (1980).

[9] V. P. Saenko and R. N. Gorbatyuk, On gerotor hydraulic machine design, *Russian Engineering Research* 24 (7) (2004) 8-14.

Soon-Man Kwon received his B.S., M.S., and Ph.D degrees in Mechanical Engineering from Yonsei University, in 1989, 1991, and 2001, respectively. Dr. Kwon is currently an Associate Professor at the Department of Mechanical Design & Mfg. Engineering at Changwon National University in Korea. Dr. Kwon's research interests are in fracture and fatigue behaviors of materials, and creative mechanism and mechanical design.

Joong-Ho Shin received his Ph.D. degree from Ohio State University in 1986. Dr. Shin is currently a Full Professor at the Department of Mechanical Design & Mfg. Engineering at Changwon National University in Korea. Dr. Shin's research interests include computer aided mechanism and mechanical design.